Maximum-entropy reconstruction of the internal magnetization density distributions in $Fe_3(Al_xSi_{1-x})$ alloys

1995 J. Phys.: Condens. Matter 7 1373

(http://iopscience.iop.org/0953-8984/7/7/018)

J. Phys.: Condens. Matter 7 (1995) 1373–1389. Printed in the UK

Maximum-entropy reconstruction of the internal magnetization density distributions in $Fe_3(Al_xSi_{1-x})$ alloys

L Dobrzynski†‡
† Institutt for Energiteknikk, PO Box 40, N-2007 Kjeller, Norway

Received 23 June 1994, in final form 9 September 1994

Abstract. Magnetization distributions in Fe_3Al, Sendust, Fe_3Si and Fe_4Si have been reanalysed by applying the model-free maximum-entropy method. The results show that in the first three alloys the magnetic moments of iron at the B sites decrease while their e_g-type asphericities increase with increasing silicon content. The asphericities at (A, C) sites are not very different from those at B sites. Compared with the situation in BCC iron, the formation of DO_3 ordering with the presence of silicon increases the number of e_g states at the Fermi level, while the opposite is true for aluminium atoms. Iron substituting for aluminium or silicon exhibits a substantially different degree of asphericity than exhibited at B sites. In the case of substitution for silicon a decrease in the magnetic moments at D sites with respect to the B sites is seen. The spatial extent of the magnetization distribution at iron sites is generally more extended than observed in pure iron.

From the purely maximum-entropy point of view, negative magnetization is not needed for the magnetic structure factor reconstruction. However, at least in the case of Sendust alloy, it is shown that such magnetization is necessary in order to obtain a sensible spatial distribution of the magnetization at the D site. It is shown that, once negative magnetization is allowed, its distribution throughout the unit cell has a localized character.

1. Introduction

The success of a model-free maximum-entropy method applied to reconstruct the spatial distributions of the magnetization densities in nickel and iron [1] enabled us to turn our attention to some problems encountered in the interpretation of magnetic form factors measured for Fe_3Al [2], Fe_3Si [3] and an almost 2:3 mixture of these two alloys, called Sendust. The results of the measurements carried out on the latter, as well as a comparison of the magnetic form factors measured for all three alloys have been presented in [4]. The following conclusions based on the results of [4] deserve to be mentioned.

(i) The spherical part of the magnetic form factors attributed to iron sites is generally narrower than the spherical part of the magnetic form factor of pure iron.

(ii) There seems to be no systematic change in the magnetic moments nor in the asphericity of the iron magnetization distributions when one proceeds from Fe_3Al through Sendust to Fe_3Si. Also, it is not clear whether there are any differences between the asphericities observed for (A, C) and for B sites; the estimated relative populations of the e_g states depend very much on the applied method of analysis. As an example, the results of [4] show that the degrees of the asphericity at the two sites, determined in [2], have almost a reversed order when the same set of data is analysed in a different way.

‡ Mailing address: Institute of Physics, Warsaw University Branch, Lipowa 41, 15-424 Bialystok, Poland.

0953-8984/95/071373+17$19.50

(iii) The magnetic form factors associated with the magnetic moments at Al/Si or D sites behave in a non-standard way, showing oscillations and achieving values exceeding unity at certain momentum transfers. The shape of these form factors deviates more and more from the 3d type when one proceeds through the series of these alloys from Fe_3Al to Fe_3Si.

In addition to these conclusions in [4], one should add that a non-centrosymmetric contribution to the spin-density distribution around (A, C) sites has been found [2] for Fe_3Si alloy.

All these features are intriguing indeed. One should bear in mind, however, that the numerical analysis performed so far for these alloys relied heavily on certain models. Also the Fourier analysis carried out in all three papers [2–4] could suffer from some ambiguities owing to the incompleteness of the experimental data sets. Only in the case of Sendust [4], have all reflections up to (444) ($(\sin\theta)/\lambda = 0.606$) been measured. In the remaining alloys, the form factor of the (531) reflection is systematically missing. The magnetic structure factors of fundamental reflections have been reported up to $(\sin\theta)/\lambda \simeq 0.9$, 0.89 and 0.83 for Fe_3Al, Sendust and Fe_3Si, respectively. However, even in this range the (642) reflection has not been measured for any of the alloys in question. In the region where $(\sin\theta)/\lambda > 0.63$ most of the superlattice reflections have not been measured for Sendust and Fe_3Si. The oldest and most complete data set for Fe_3Al [2], collected up to $(\sin\theta)/\lambda \simeq 0.9$, shows only the occasional absence of experimentally determined magnetic form factors for the superlattice reflections. Of course, in addition to the lack of some data, the usual series termination errors appearing in the Fourier analysis can superimpose and increase the number of spurious details in the magnetization density maps.

In the light of all these uncertainties, the use of a model-free approach could clarify the situation in these interesting compounds.

As has been shown in [1], one can find, by means of the maximum-entropy algorithm, maps of positive- and negative-magnetization distributions throughout the unit cell. These maps are generally believed to be much less sensitive to the cut-off errors and incompleteness of the data than is the Fourier method. Moreover, this approach does not use any of the magnetic form factors calculated for a free atom or ion and subsequently fitted with a certain number of parameters to the observed magnetic structure factors.

Technically, the problem of finding the maps for the alloys in question is more difficult than for iron or nickel because of the almost doubled unit-cell volume in the case of alloys. In order to achieve the same accuracy, one should carry out the analysis on a $128 \times 128 \times 128$ grid, which would require a computer memory eight times larger and a correspondingly enhanced CPU time. The calculations presented in this paper have been carried out for a grid of $64 \times 64 \times 64$ pixels in the unit cell, i.e. the same as used in [1].

The entropy used had the form given by Papoular and Gillon [5]. The software package MEED [6], modified to deal with positive and negative scattering lengths and supplied kindly by Professor M Sakata, had to be modified in order to make use of the algorithms [5]. In one case (Fe_4Si, see section 2), extra care was taken in order to obtain an even distribution of residuals, but it was checked that qualitatively the maps of magnetization densities obtained are not particularly sensitive to this distribution.

2. Structure and magnetic moments

The crystal structure of the alloys is of the $D0_3$ type. It is composed of four interpenetrating FCC lattices shifted by one quarter of the main diagonal with respect to each other.

The positions of the iron atoms are $(0, 0, 0)$ + FCC translations (so-called B sites), $(\frac{1}{4}, \frac{1}{4}, \frac{1}{4})$ + FCC translations (C sites), $(\frac{3}{4}, \frac{3}{4}, \frac{3}{4})$ + FCC translations (A sites), whereas the positions $(\frac{1}{2}, \frac{1}{2}, \frac{1}{2})$ + FCC translations (D sites) are occupied by aluminium or silicon only, if perfect ordering is achieved. The abbreviations of the positions may vary depending on the chosen origin of the unit cell. What is important, however, is that the B sites are surrounded by eight iron atoms in a way very similar to the coordination in pure iron, whereas iron at two symmetry-equivalent A and C sites has four iron (B) and four aluminium/silicon (D) nearest neighbours. The sequence of sites in the consecutive nearest-neighbour shells is presented in table 1.

Table 1. Composition of the sixth-nearest-neighbour shells around each site in the $D0_3$ type of structure.

	Composition for the following shell numbers					
Site	1	2	3	4	5	6
(A, C)	4B, 4D	6(A, C)	12(A, C)	12B, 12D	8(A, C)	6(A, C)
B	8(A, C)	6D	12B	24(A, C)	8D	6B
D	8(A, C)	6B	12D	24(A, C)	8B	6D

In practice, certain B–D disorder may be present, which almost always happens in Fe_3Al, an alloy difficult to order completely. Because of this situation, some iron atoms occupy D sites. One can expect that they will possess magnetic moments comparable with those at B sites because the nearest-neighbour surroundings of both positions are identical. Moreover, the first two coordination spheres around D sites are identical with those of pure BCC iron.

In accordance with [4], there is no systematic trend in the values of magnetic moments at (A, C) sites nor at B sites. On the average, the spherical magnetic moments have been determined to be 2.5 μ_B at B sites and 1.12 μ_B at (A, C) sites. The relative occupancies of e_g states have been estimated to be 0.56 and 0.57, respectively. Although some trend in the dependence of these values on the relative concentrations of aluminium and silicon atoms seems to occur, the statistical errors did not permit an unambiguous determination.

On the other hand, the magnetic moments attributed to D sites has been reported [4] to vary in a systematic way from 0.23 μ_B in Fe_3Al through 0.06 μ_B in Sendust to 0.02 μ_B in Fe_3Si. This has been interpreted as a tendency of Si to form well bonded states which are difficult to polarize. As has been stated already, the shape of the magnetic form factors which could be attributed to the D sites does not resemble that known for iron, implying that electrons other than d electrons may be responsible for the magnetization at these sites. In order to clarify this point, we analysed also the data [3] for the Fe_4Si alloy containing 20 at.% of Si only. With no silicon present at either B or (A, C) sites, 20% of the D sites must be populated in this alloy by iron. This should allow one to gain a better understanding of the behaviour of iron at these sites.

3. Results

The magnetic structure factors of Sendust [4] have been used to test whether one can reconstruct them by assuming a strictly positive magnetization density in every pixel. This should be possible, as it was also in the case of iron and nickel [1]. However, because the

presence of negative-magnetization regions in the unit cell seems rather well established in ferromagnetic 3d metals, the main effort was concentrated on retrieving the measured magnetic structure factors by assuming that the total magnetic moment consists of a positive and a negative part, each having its own spatial distribution. Thus, the influence of a pre-assumed level α of negative moment ($\mu_{\text{negative}} = \alpha\mu_{\text{total}}$) has been studied for every alloy. In particular, the maps have been calculated for a negligibly small and physically almost unmeasurable magnetic moment when $\alpha = 0.005$. The maps obtained have been compared in all cases with the others calculated for $\alpha = 0.1$. In all four cases the most significant details seen for $\alpha = 0.1$ survive when it is reduced to 0.005.

3.1. Fe_3Al

Although the maximum-entropy routine converged and produced maps which resulted in calculated structure factors agreeing with the measured values within the χ^2 test, it should be noted that the main contribution to χ^2 comes from the fundamental reflections. For about half of them the deviations are larger than the statistical error of measurements. This could be due to the nature of the maximum-entropy algorithm itself, as noted earlier [7]. An uneven distribution of residuals was also present in the reconstructions of iron and nickel data [1]. However, one cannot exclude that the deviations observed for Fe_3Al could be due to some inaccurate determination of the secondary extinction in this pioneering experiment [2] from 1961.

The (100) sections of the positive part of the magnetization density maps, calculated with $\alpha = 0.005$ for $Z = 0$ and $Z = \frac{1}{4}$ are shown in upper left-hand corners of figures 1 and 2. Contours are drawn in the 0.1 fraction of the maximum amplitude of the distribution (cf figures 5 and 6). It is seen that the magnetization density is localized well around the B (corner and central sites in this section) and D (midedge) positions (figure 1). A similar situation holds for (A, C) sites (figure 2; in order to determine the scale see figure 4 later). To magnify the effect of the magnetization observed at aluminium (D) sites, the magnetization density map showing the densities below 0.2, which is roughly the maximum value observed at D sites in all but Sendust alloy, is presented in figure 3, which displays the results of calculations with $\alpha = 0.1$. Note that this figure shows the $Z = \frac{1}{2}$ section of the (100) plane; so D sites are the central and corner sites. Comparing the maps from figure 3 with similar maps calculated for $\alpha = 0.005$, one can easily convince oneself that all the qualitative details are independent of α.

The magnetization distributions have definite asphericities, which are illustrated better in figures 4–6, showing the distributions around every site. What is interesting to note is that at both iron sites there is an apparent symmetry of e_g type, while at D sites the symmetry changes to a t_{2g} type. At the same time, the spatial extent and overall shape of the magnetization distribution at the D site are contracted with respect to those observed at typically iron sites. As we also see from the last three figures, the magnetization densities show some depletion at the centres, the effect observed earlier for nickel and iron [1]. Here this effect is weaker, which is due to both the limited range of $(\sin\theta)/\lambda$ covered and the larger volume per pixel. An increase in α makes this depletion smaller. This is due to the maximum-entropy property of delivering a broader distribution with increasing lack of information about this distribution.

It is also interesting to compare the asphericity observed at the B site with that observed in BCC iron. This latter is displayed in figure 7. Such a comparison shows that the e_g states in iron are relatively more populated than similar states at the B site, which has an identical nearest-neighbour shell. This, together with a comparable e_g character of the iron moment

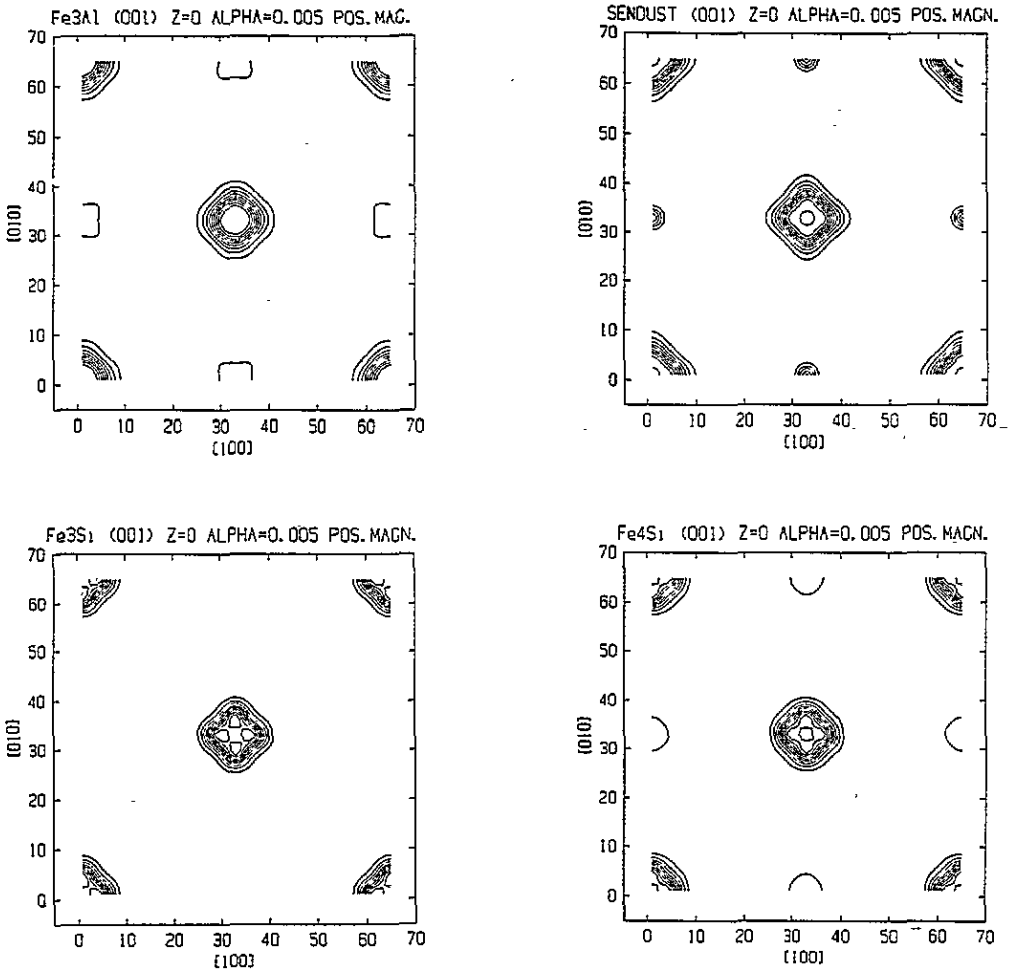

Figure 1. Magnetization distribution in the (100) plane for the section $Z = 0$, calculated with $\alpha = 0.005$. The contours are drawn every tenth of the maximal densities observed at B sites; cf figure 5.

at (A, C) sites and reversed symmetry at D sites, indicates the importance of the next shells of neighbours on the magnetic moment formation.

Regions of negative magnetization have been found in some localized portions of the unit cell. With the larger negative moment required, the corresponding maps of negative-magnetization densities become more diffuse. This effect, however, is once again due to spreading our uncertainty of a true level of the negative moment over the unit cell and may not reflect the true physics of the problem. Similarly to the case of iron and nickel, the magnetic structure factors corresponding to the negative magnetization oscillate. Their absolute values, however, are usually within the experimental error bars. The maps of negative density calculated with $\alpha = 0.1$ of the $Z = 0$ section of the (001) plane are shown in figure 8. As mentioned before, although the shapes of the maps depend on the pre-assumed value of the negative magnetization, the main features do not depend on α. The distribution of contours in all maps is presented always in tenths of the largest negative

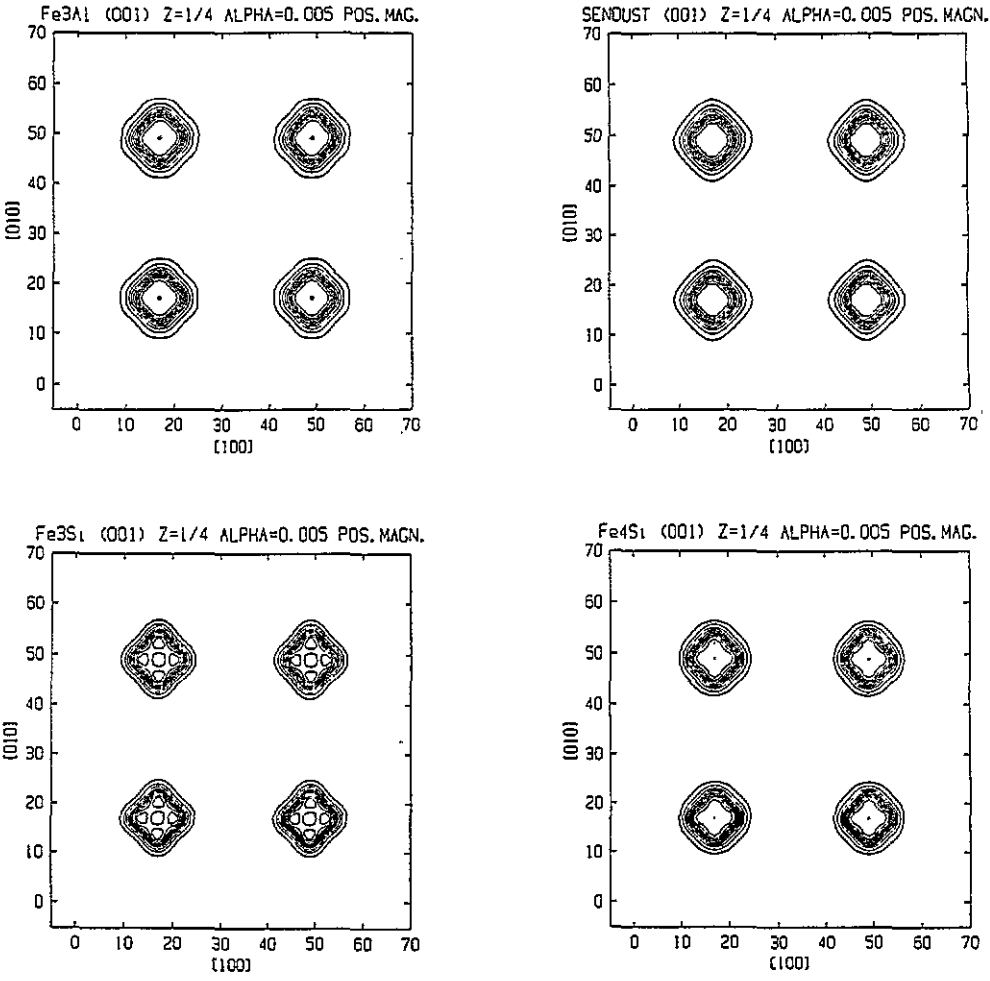

Figure 2. Same as figure 1 for the section $Z = \frac{1}{4}$.

value. An interesting observation is that the overall shape of the negative-magnetization distribution is quite far from that observed for pure iron [1, 9].

3.2. Sendust

The exact composition of this crystal is $Fe_{2.94}Al_{0.38}Si_{0.68}$. This means that about 6 at.% Al and/or Si atoms must occupy iron positions. This is indeed the case and, as found earlier [8], the excess non-ferrous atoms go preferentially to B sites. The excess aluminium atoms cause a substantial decrease in the average magnetic moment. Its measured value, 4.44 μ_B [4], can be compared with the value expected for the $Fe_3Si_xAl_{1-x}$ alloy with $x = 0.68$ and the change in the magnetization in Fe–Al ordered alloys [10] when one goes from 25 to 27 at.% Al. Such a comparison shows that, at least in this concentration region, the aluminium atoms act in a similar way in the absence and in the presence of silicon.

In analysing the form-factor data from [4] we had to correct for an obvious misprint in the paper, in which the Miller indices should read (840) instead of (640).

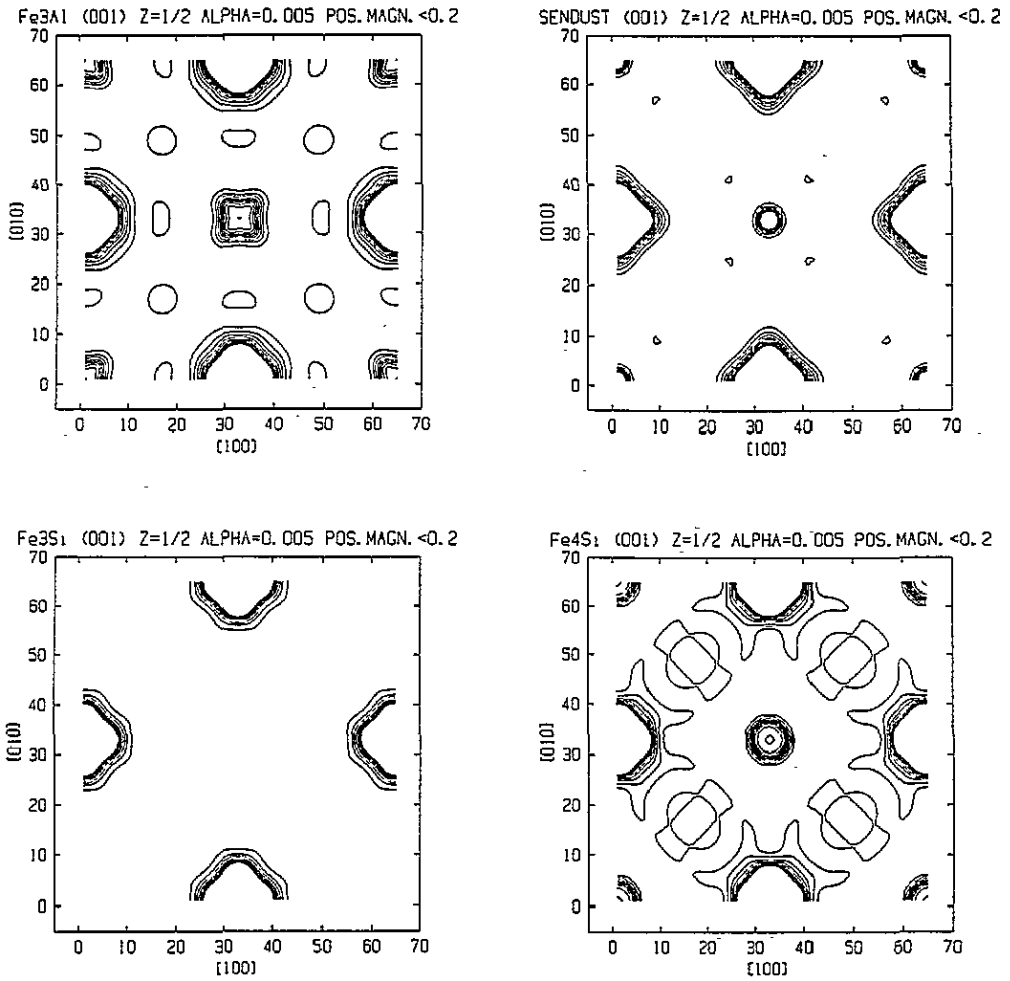

Figure 3. Same as figure 1 for the section $Z = \frac{1}{2}$ and magnetization densities below 0.2, calculated with $\alpha = 0.1$.

The magnetic structure factors were reproduced satisfactorily by the maximum-entropy algorithm. Although there are few reflections which carry most of the weight of χ^2, these reflections, however, are of all types, in contrast with the situation found for Fe_3Al.

The magnetization density distributions along two high-symmetry directions around every site are shown in figures 4–6, which collect the results obtained for all the samples in question. It can be seen that the asphericity at the B sites is quantitatively very close to that found for pure iron. The distribution at the D site, however, is spherically symmetric, at least close to the nucleus, and the spatial distribution of the magnetization at the D site is very contracted with respect to those at the remaining sites. In fact, this distribution contracts greatly when the level of negative magnetization is decreased below $\alpha = 0.1$. Therefore, if the magnetic moment observed at this site is due to iron atoms whose magnetization density distribution should not differ much from those observed for B sites, we must conclude that the parameter α indicating the level of negative magnetization must be at least as large as 0.1.

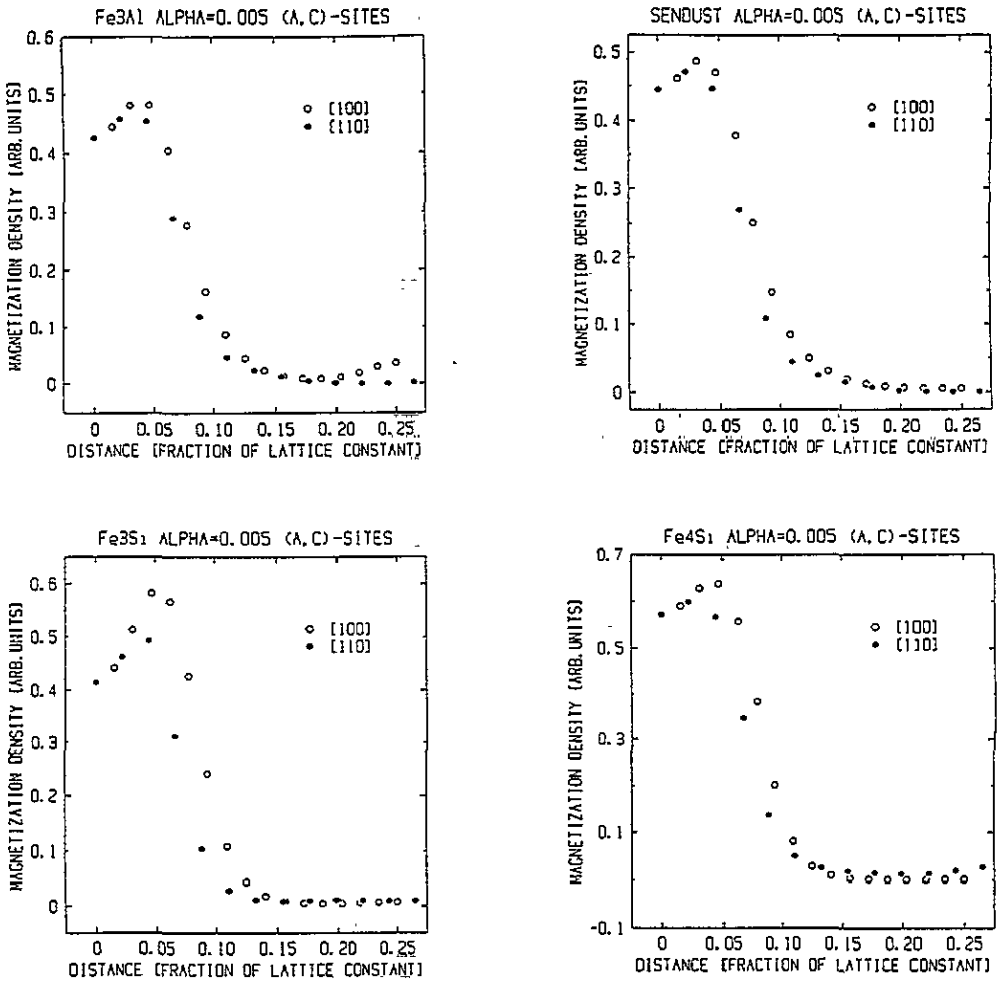

Figure 4. Magnetization density at the (A, C) sites along two high-symmetry directions; $\alpha = 0.005$.

In addition, a small but easily visible peak appears in between the D and (A, C) sites in a distance of approximately $0.17a$ from the D sites, where a denotes the lattice constant. This peak is also visible along the [111]-type directions around the D site and drops below the significance level along the [100]-type directions. Its appearance as well as its intensity turn out to be independent of the prior assumption as to whether there is or is not a negative moment in the alloy.

The negative-density maps show, as in the case of Fe_3Al, much structure at every section. They are, however, very different from those observed for the Fe_3Al alloy. We shall discuss these densities in section 4.

3.3. Fe_3Si and Fe_4Si

In order to perform the analysis, we have averaged first the data given in [3] for two different samples of each composition. Except for some of the fundamental reflections which have been measured on different samples and sometimes on two extra equivalent reflections, in all

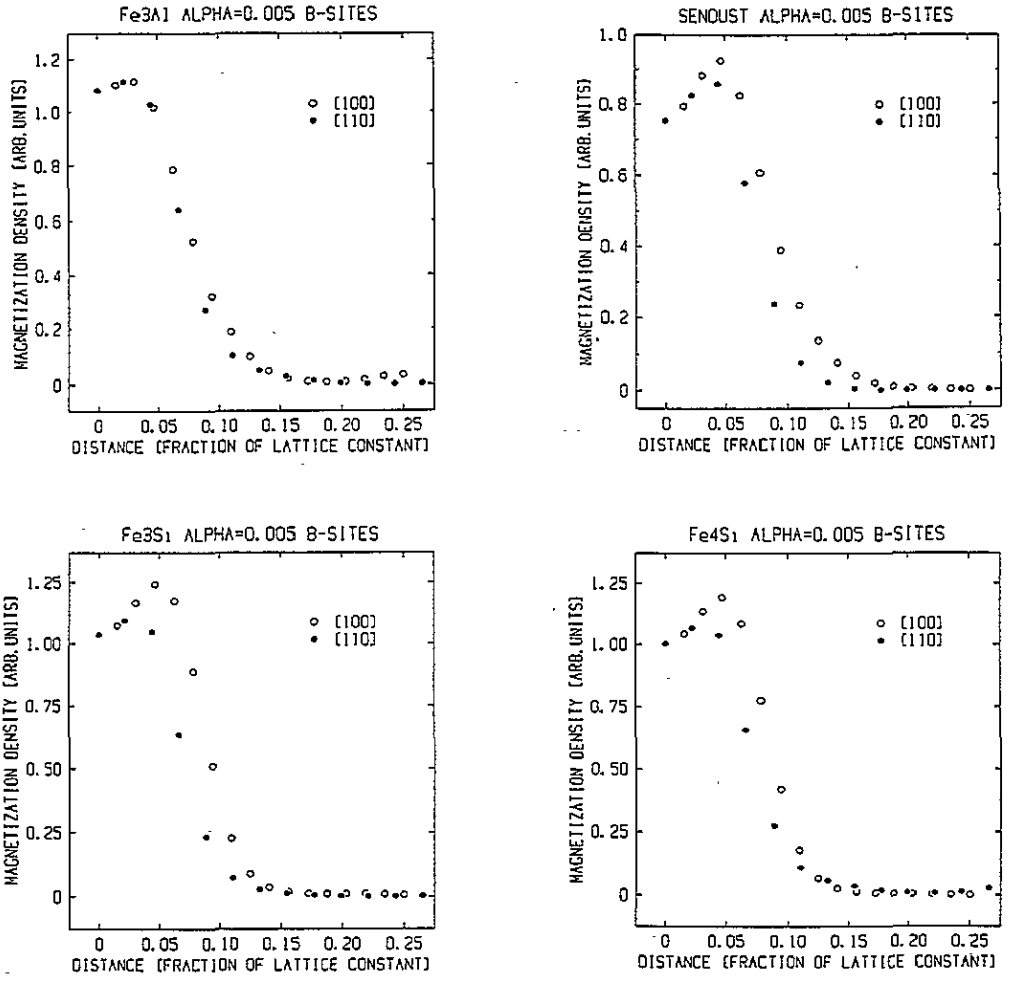

Figure 5. Same as figure 4 for the B sites.

the remaining cases we have taken the values of the experimental errors determined before (rather substantial) correction for secondary extinction in these samples. (The published data for Fe_3Si contain a misprint in the value of the magnetic structure factor for the (111) reflection. Instead of the published 1084 (in units of 10^{-15} cm) it should read 1840; this can be inferred from the values of the magnetic moments.)

As was stated in the introduction, the presence of iron at D sites in Fe_4Si should allow one to understand the effect that can be expected when iron substitutes for silicon. Essentially the positive-magnetization distributions observed at these sites in this alloy and in Fe_3Al (in which iron appears because of the B–D disorder) exhibits two notable differences: firstly the distribution is more compact in Fe_4Si than in Fe_3Al, and secondly the magnetization in Fe_4Si exhibits very weak e_g (almost spherical) symmetry, while that in Fe_3Al is apparently of t_{2g} type. Because the peak values are quite comparable, and the amount of iron at D sites should be larger in the Fe_4Si alloy, these results show that either the magnetic moment of iron at the D site is much smaller in Fe_4Si than in Fe_3Al or the non-ferrous atoms assume some magnetic moments. We also note that the spatial extent of

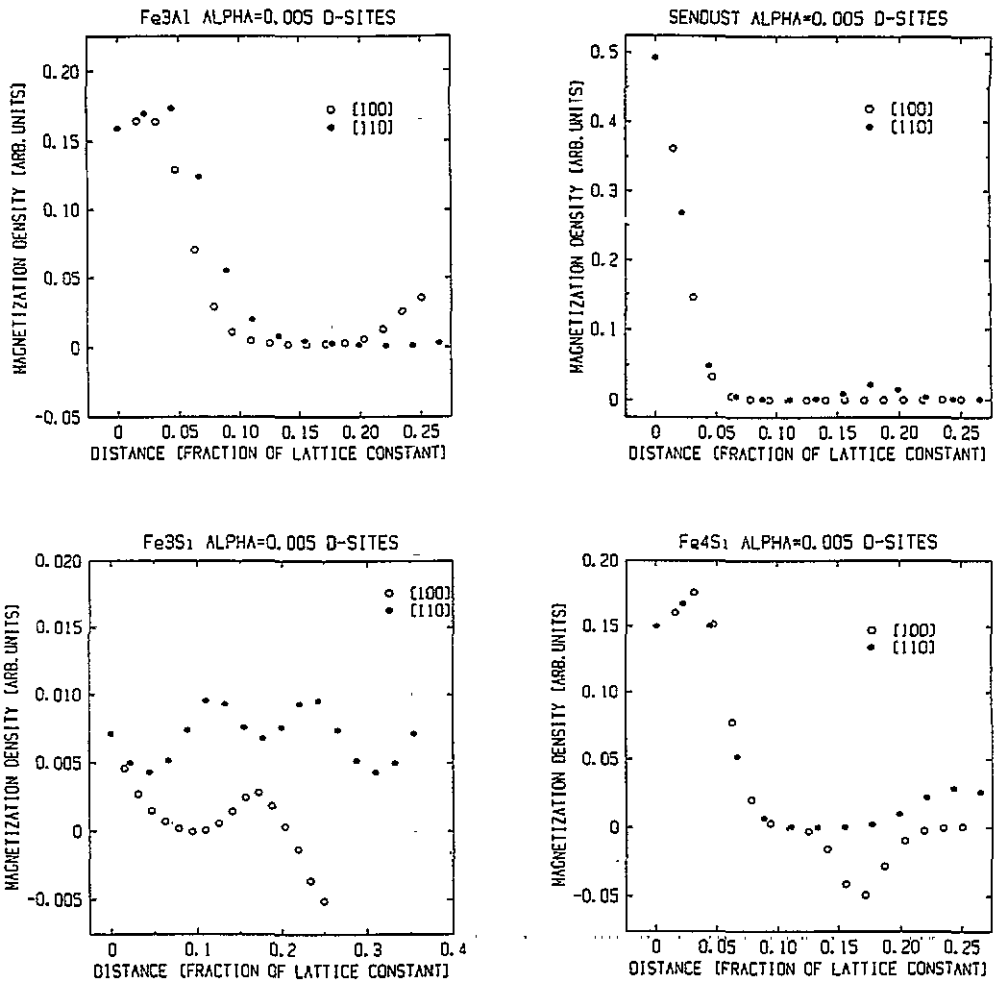

Figure 6. Same as figure 4 for the D sites.

the positive magnetization at the D site in Fe_4Si is smaller than at the B site. This time, however, in contrast with the case of Sendust, an increase in α does not help and makes the distribution even narrower.

Apparently a different situation is met in Fe_3Si. From the measured silicon concentration in this alloy (24.3 at.%), one expects that about 2.5% of D sites will be populated by iron. It is easy to scale the distribution presented in figure 5 by 0.025 and to compare the result with that displayed in figure 6. As will be discussed in the next section, the magnetic moment observed at D sites of Fe_4Si is substantially lower than expected. We see that also, in Fe_3Si, one can hardly see any trace of the presence of iron at D sites.

A very characteristic feature of the Fe_4Si data for the surroundings of the D site is the appearance of negative magnetization along the [100] direction, and a positive lobe at the middle of the D–D bond. This positive lobe is also very visible in the Fe_3Si alloy, for which the magnetization distribution at this site is highly non-trivial. It cannot come from any B–D disorder, because such a disorder was not detected. However, because the absolute level of this magnetization is very low indeed, its significance is difficult to assess.

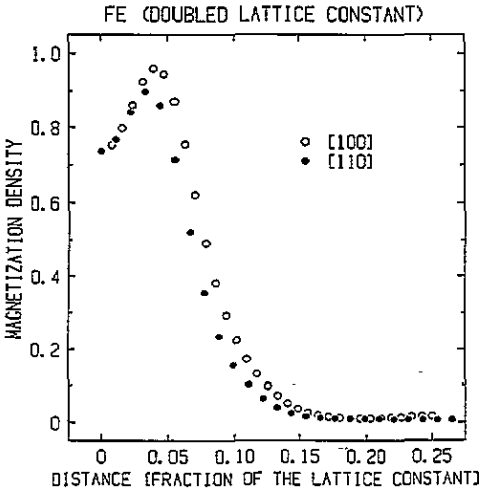

Figure 7. Magnetization density distribution along [100] and [110] directions in BCC iron. In order to have the same units on the abscissa, the lattice constant of iron was doubled.

A similar situation concerns another interesting feature seen in the magnetization distribution along the [111] direction, where some pile-ups of magnetization are observed along the D–(A, C) and (A, C)–B bonds.

This as well as other small features can in principle be artefacts owing to inaccuracies introduced by the maximum-entropy algorithm itself. In this context we were particularly concerned with non-even distribution of residuals. As an example, in the case of Fe_4Si, almost all χ^2 is given by the residual at the (220) reflection. Therefore, independent calculations which involved so-called E^2 statistics [11] have additionally been carried out. The effect that is produced if the reflections showing the largest residua ('outliers') are not taken into calculations has also been determined. In the latter case, the usual situation is the appearance of other 'outliers' not present before. Nevertheless, the final outcome of this analysis is that, although the amplitude of the small maxima in the magnetization density maps may vary slightly, depending on the procedure (the χ^2 or E^2 case), the qualitative image of the distribution is sensitive neither to the assumed level of negative magnetization nor to the statistics used. It can still depend on the fineness of the grid used in computations but this, for computer memory and time reasons, we have not been able to check.

Table 2. Magnetic moments per site calculated within a cube with a side of one quarter of the side of the unit cell.

	Magnetic moment (μ_B)						
		$\alpha = 0.005$			$\alpha = 0.1$		
Compound	Total	A site	B site	D site	A site	B site	D site
Sendust	4.437	0.94	1.84	0.087	0.95	1.82	0.090
Fe_3Si	4.793	0.94	1.89	0.033	0.93	1.88	0.035
Fe_3Al	5.084	0.92	2.04	0.317	0.91	2.03	0.310
Fe_4Si	5.456	1.02	1.92	0.124	1.02	1.92	0.105

4. Discussion

4.1. Magnetic moments

From the calculated magnetization densities the magnetic moments which can be attributed to every site can be deduced. Table 2 present these moments estimated within a cube with a side of 16 pixels, i.e. about 14.1 nm. The volume of this cube is the same as that of a sphere with a radius of about 8.8 nm. This relatively small volume has been chosen in order not to deal with some diffuse moments which when present in a system may be due to electrons other than d electrons. The calculations confirm the observation of [4] that the magnetic moment at the D site is the largest for Fe_3Al and the smallest for Fe_3Si. Also the magnetic moment at the B site is larger in the latter than in the former alloy. The moments at (A, C) sites are independent of the relative proportions of silicon and iron. Similar results are obtained for the magnetic moments calculated within spheres with radii of approximately 7.1 nm and 9.8 nm (table 3). These moments are weakly sensitive to the change in α from 0.005 to 0.1.

Table 3. Magnetic moments per site calculated within spheres with radii of approximately 7.1 nm and 9.8 nm. $\alpha = 0.005$.

	Magnetic moment (μ_B)						
		$R = 7.1$			$R = 9.8$		
Compound	Total	A site	B site	D site	A site	B site	D site
Sendust	4.437	0.97	1.90	0.034	1.18	2.24	0.070
Fe_3Si	4.793	0.92	1.92	0.012	1.11	2.20	0.056
Fe_3Al	5.084	0.90	2.10	0.314	1.14	2.57	0.371
Fe_4Si	5.456	0.99	1.90	0.097	1.21	2.29	0.085

The case of Fe_4Si is somewhat different. The moments at (A, C) and B sites increase with respect to the moments observed in Fe_3Si. We confirm the observation of Moss and Brown [3] of the surprisingly low value of the magnetic moment at D site. From the composition of the alloy it follows that about 20% of iron atoms should reside at D sites. Because of the nearest-neighbour surroundings (see table 1), one expects that the magnetic moment of iron should not differ much from that at the B site. Therefore it is expected that the total magnetic moment at the D sites in Fe_4Si should be of the order of 0.4 μ_B. However, it is about four times smaller. Because it is hard to believe that an inaccuracy in the determination of the concentration of silicon in this sample should be blamed for such a large effect, one has to accept it as a physical fact. The negative polarization of silicon and/or strong hybridization effects would offer the easiest explanation of the observed discrepancy. As is seen from figure 6, in the case of Fe_3Si the magnetization at the silicon site varies rapidly close to the atom centre. Its value, however, is so small that one has to agree with the supposition of [4] that silicon tries to preserve its bonding character and resists magnetic polarization. Such a polarization can appear when the bonds are broken by iron substituting for silicon, as is the case for the Fe_4Si and Sendust alloys. The asphericity of the moments formed at D and B sites are also very different.

In the case of the Fe_3Al alloy the value of the magnetic moment at the D site is relatively large and can be explained as coming from the contribution of iron located at this site. If the magnetic moment of iron were equal to that at the B site, then, in accordance with the data presented in table 2, this would mean that about 13.5% of iron atoms reside at the D

site. This value is not far from the expectations based on the B–D disorder observed for this sample. The iron residing at the B site must then have magnetic moment of about 2.38 μ_B. For the values calculated within spheres with radii of 7.1 nm and 9.8 nm, one arrives at 13.0% and 12.6%; so we see that the estimated amount of disorder is not particularly sensitive to the integration volume. This is naturally not the case for the magnetic moments, which appear to be 2.14 μ_B and 2.95 μ_B, respectively.

Because, in Sendust, 6 at.% of excess aluminium atoms are located in B positions, the magnetic moment of iron at these positions appears to be 1.96 μ_B, 2.02 μ_B and 2.38 μ_B for the integration over the cube and the two spheres, respectively.

Comparing these results with those obtained for Fe_3Si, we see that irrespective of the integration volume the calculated magnetic moments of iron at B sites systematically decrease when the amount of silicon increases (table 3). We have no theoretical grounds for expecting that this change should be linear. Nevertheless, assuming that it is, one finds the magnetic moment of iron in Sendust to be a few per cent lower than this dependence could indicate. Such a situation can, however, arise from the presence of excess Al atoms. Indeed, the excess aluminium atoms in Sendust must cause a rather strong decrease in the iron moments. Whether it takes place on both sites or on one only is not easy to assess. From [10] it follows that the 6 at.% of excess Al atoms can reduce the moments by about 13%. On the other hand, our analysis indicates that the magnetic moment of iron at the A site of Sendust is a little larger than that in Fe_3Al and Fe_3Si. This can suggest that the excess aluminium atoms cause a decrease in iron moments mainly at B sites.

4.2. Asphericities

One can try to quantify the asphericity by decomposing the calculated magnetization distributions into symmetry-allowed densities. However, this is impossible to do without assuming a certain model of the distribution, which we try to avoid. Therefore we decided to compare the magnetic moments obtained as above with the moments which would have been obtained if the spatial distribution were as found for the [100] direcion in these alloys. The results are presented in table 4.

Obviously, the e_g-like moments calculated in this way are unphysically large. Nevertheless their behaviour in different alloys should reflect the real trends. That this is the case can also be checked by making difference maps for normalized distributions. One can also compare the ratios of these moments and those presented in tables 2 and 3. We conclude that there is a definite trend for the B sites. With increasing silicon content the asphericity increases. In the case of (A, C) sites the e_g-type moment is definitely larger in Fe_3Si than in Fe_3Al, but the degree of asphericity is lower in Sendust than in Fe_3Al.

In the case of Fe_4Si, one can note that the excess iron atoms cause more or less similar lowering of the e_g-type asphericity at both sites. Because in the limiting case of increasing iron concentration one arrives at BCC iron, this leads to the conclusion that silicon atoms in DO_3-type structures must enhance the predominant location of e_g-type electrons close to the Fermi level in the iron-like, i.e. B, sites. Conversely, the opposite effect should hold when aluminium atoms are ordered in D sites.

The weak magnetization observed at the D site in the Fe_3Al alloy is unexpectedly of t_{2g} type, very weakly e_g type in Fe_4Si and spherically symmetric in Sendust. This feature accompanies the general narrowing of these distributions, which is another unexpected and hard-to-explain effect. (On the other hand, the observed narrower distribution at D sites compared with (A, C) and B sites agrees with the conclusion of [4] that the ferrous sites in the considered alloys exhibit a broader distribution than observed in pure iron.) In the

Table 4. Magnetic moments of iron and their relative increase if isotropic densities obtained for [100]-type directions are substituted for the true densities calculated within spheres with radii of approximately 7.1 nm and 9.8 nm.

	$R = 7.1$				$R = 9.8$			
	A site		B site		A site		B site	
Compound	Magnetic moment (μ_B)	Relative increase	Magnetic moment (μ_B)	Relative increase	Magnetic moment (μ_B)	Relative increase	Magnetic moment (μ_B)	Relative increase
Fe_3Al	0.90	1.39	2.41	1.21	1.14	1.19	2.95	1.31
Sendust	0.97	1.22	2.02	1.49	1.18	1.60	2.38	1.27
Fe_3Si	0.92	1.75	1.92	1.75	1.11	1.70	2.20	1.61
Fe_4Si	0.99	1.46	1.90	1.54	1.21	1.40	2.29	1.28

case of the Fe_3Si alloy, the distribution of magnetization at the D site is so peculiar that it makes no sense to discuss it in terms of t_{2g} and e_g states.

The drastically different symmetry of the magnetization distributions at D sites is a spectacular effect indeed. As was mentioned already, the first two coordination spheres around the D site are identical with those for BCC iron. The fact that they do not succeed in creating the same symmetry of the spatial distribution of magnetization indicates how important are more distant atoms for the formation of the band structure.

4.3. Interstitial regions

The maps of positive-magnetization density reveal that in Fe_3Al and Fe_4Si a small maximum is seen in the middle of the Al–Al (Si–Si) bond. In Sendust and in Fe_3Si alloys this maximum splits into two maxima lying closer to the D sites. A certain tendency to such a splitting can also be inferred from the maps obtained for the Fe_4Si alloy. Therefore we associate this phenomenon with the presence of silicon. The maps shown in figure 3 are convincing in showing what a difference the aluminium makes with respect to silicon in the alloys. In particular, an extra positive lobe is seen close to B sites along the B–D bond in Fe_3Al. In addition, in the case of the Fe_4Si alloy, a similar lobe close to B and extending towards (A, C) sites is seen. As mentioned before, it is not easy to prove that small details seen on the maps produced by the maximum-entropy algorithm are not due to the algorithm itself. In this context we shall only say that we have run the data of iron as if it possessed a DO_3 type of structure. The original data of Shull and Yamada [14] have been shortened, so as to be in the same range of $(\sin\theta)/\lambda$ as the other data used by us. We have run the data for iron in two versions. In the first, 16 'fundamental' reflections only have been given as input. In the second, we have added 30 zero-valued superstructure reflections of (111) and (200) types. As a result we could see that no spurious details were produced, and the magnetization density distribution did not differ from that obtained in [1]. Therefore we are inclined to think that in the form factors studied in the present paper there must be evidence for these positive lobes observed on the maps. Nevertheless, there is no doubt that an analysis of the variance of the reconstructed density distributions should be carried out in the future. At the moment it could not be performed for purely technical reasons.

The negative-magnetization density distributions in the (001) plane at $Z = 0$ and in the (110) plane are shown in figure 8. As can be seen, there is quite a variety in the behaviours of this magnetization. The common feature is a negative dip appearing along the [100]-type directions around D sites. In the case of Fe_3Al, other dips of negative magnetization appear around the Al–Al bonding line. As we have said already, the presence of negative magnetization is not necessary for the maximum-entropy reconstruction as such. What indicates the justification of its introduction is the observation of an apparent narrowing of the magnetization distribution of iron residing at D sites, especially in the case of Sendust. Because it is hard to believe that having the nearest- and next-nearest-neighbour surroundings (see table 1) identical with those for BCC iron, the spherical part of the distribution will be very different from that observed for iron (figure 7), we find this as the only but important argument in favour of the presence of the negative magnetization in all the alloys studied here. Iron does not show up at the D sites in Fe_3Si alloy, and therefore, in this alloy the situation concerning the negative magnetization cannot be solved unambiguously. Clearly, an experiment on magnetic Compton scattering [12, 13] would be of great importance here, as it would indicate whether a negative conduction electron polarization should exist in this alloy.

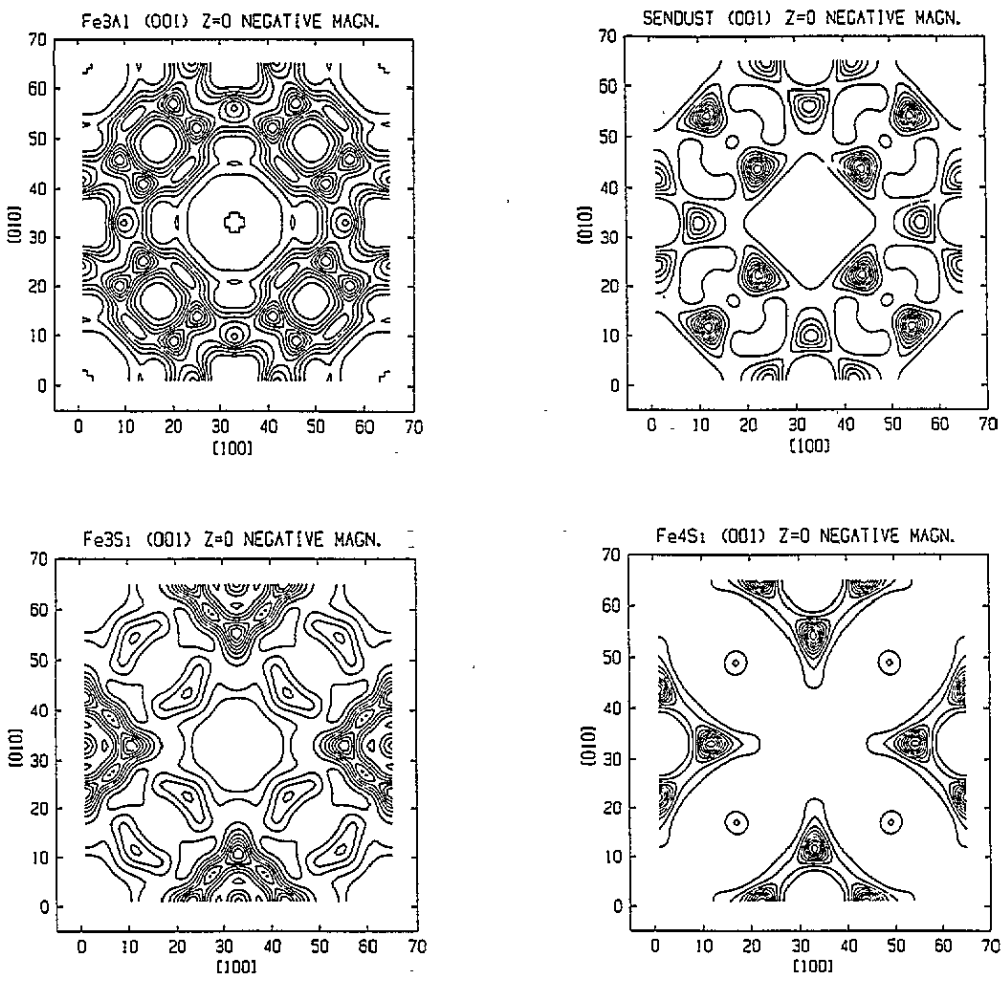

Figure 8. Negative-magnetization densities in the (100) plane, for the section $Z = 0$; $\alpha = 0.1$. Similarly to figures 1–3 the contours are drawn every tenth of the maximal value of the density. These values are the following: for Fe_3Al, 0.0072 in pixel (8, 20) and other symmetry related; for Sendust, 0.020 in pixel (12, 12) and other symemtry related; for Fe_3Si, 0.0099 in pixel (1, 23) and other symmetry related; for Fe_4Si, 0.0354 in pixed (1, 22) and other symmetry related.

5. Summary

The magnetization density distributions of some Fe–Si–Al alloys with $D0_3$-type structure have been analysed by the same method, namely the maximum-entropy method. The most important features, which have not been found when the Fourier analysis or magnetic form factor fitting procedures were employed are the following:

(1) the depletion of the magnetizations at the nuclei positions;

(2) apparently different asphericities and amounts of narrowing of the distributions at the D sites compared with the B sites;

(3) systematic change in magnetic moments of iron atoms at the B sites with silicon content and lack of such systematics for A sites when one proceeds from Fe_3Al to Fe_3Si;

(4) an opposite influence of silicon and aluminium atoms on the asphericity of iron at the B sites;

(5) a sample-dependent structure in the negative-magnetization distribution once its presence is postulated (the features are smeared out with an increase in the level of negative magnetization);

(6) very weak magnetic polarizability of silicon sites and apparent depletion of the magnetic moment of iron at the silicon (D) site.

Acknowledgments

I wish to express my thanks to colleagues at the Institutt for Energiteknikk for their hospitality, help and creation of excellent conditions for carrying out research. Particular thanks are due to Professor Tormod Riste for a critical reading of the manuscript. Special thanks are due to Professor M Sakata for presenting me with the MEED package, and guidance in calculations. The collaboration with Dr R Papoular is also greatly acknowledged. Professor F Sacchetti is thanked for his critical reading of the manuscript and useful comments

The work was partly sponsored by the State Council of Research, Poland, through the grant 2 0990 91 01.

References

[1] Dobrzynski L, Papoular R J and Sakata M 1995 *J. Magn. Magn. Mater.* 140–4
[2] Pickart S and Nathans R 1961 *Phys. Rev.* **123** 1163
[3] Moss J and Brown P J 1972 *J. Phys. F: Met. Phys.* **2** 358
[4] Dobrzynski L, Petrillo C and Sacchetti F 1990 *Phys. Rev.* B **42** 1142
[5] Papoular R J and Gillon B 1990 *Neutron Scattering Data Analysis 1990 (Inst. Phys. Conf. Ser. 107* (Bristol: Institute of Physics) p 101
[6] Sakata M, Uno T, Takata M and Howard Ch J 1993 *J. Appl. Crystallogr.* **26** 159
[7] Jauch W and Palmer A 1993 *Acta Crystallogr.* A **49** 590
[8] Dobrzynski L, Giebultowicz T, Kopcewicz M, Piotrowski M and Szymanski K 1987 *Phys. Status Solidi* a **101** 567
[9] Shull C G and Mook H A 1966 *Phys. Rev. Lett.* **16** 186
[10] Shull R D, Okamoto H and Beck P A 1976 *Solid State Commun.* **20** 863
[11] Reiter J 1992 *J. Comput. Phys.* **103** 169
[12] Cooper M J, Laundy D, Cardwell D A, Timms D N, Holt R S and Clark G 1986 *Phys. Rev.* B **34** 5984
[13] Tanaka Y, Sakai N, Kubo Y and Kawata H 1993 *Phys. Rev. Lett.* **70** 1537
[14] Shull C G and Yamada Y 1962 *J. Phys. Soc. Japan* **17** Suppl. BIII 1